NIST Technical Note 1968

Pool Boiling of Low-GWP Replacements for R134a on a Reentrant Cavity Surface; Extensive Measurement and Analysis

Mark A. Kedzierski
Lingnan Lin
Donggyu Kang

This publication is available free of charge from:
https://doi.org/10.6028/NIST.TN.1968

National Institute of Standards and Technology
U.S. Department of Commerce

NIST Technical Note 1968

Pool Boiling of Low-GWP Replacements for R134a on a Reentrant Cavity Surface; Extensive Measurement and Analysis

Mark A. Kedzierski
Lingnan Lin
Donggyu Kang
Energy and Environment Division
Engineering Laboratory

This publication is available free of charge from:
https://doi.org/10.6028/NIST.TN.1968

October 2017

U.S. Department of Commerce
Wilbur L. Ross, Jr., Secretary

National Institute of Standards and Technology
Kent Rochford, Acting NIST Director and Under Secretary of Commerce for Standards and Technology

National Institute of Standards and Technology Technical Note 1968
Natl. Inst. Stand. Technol. Tech. Note 1968, 41 pages (October 2017)
CODEN: NTNOEF

This publication is available free of charge from:
https://doi.org/10.6028/NIST.TN.1968

Pool Boiling of Low-GWP Replacements for R134a on a Reentrant Cavity Surface; Extensive Measurement and Analysis

M. A. Kedzierski, L. Lin, and D. Kang
National Institute of Standards and Technology
Gaithersburg, MD 20899

ABSTRACT
This paper quantifies the pool boiling performance of R134a, R1234yf, R513A, and R450A on a flattened, horizontal Turbo-ESP surface. The study showed that the boiling performance of R134a on the Turbo-ESP exceeded that of the replacement refrigerants for heat fluxes greater than 20 kWm^{-2}. On average, the heat flux for R1234yf and R513A was 16 % and 19 % less than that for R134a, respectively, for R134a heat fluxes between 20 kWm^{-2} and 110 kWm^{-2}. The heat flux for R450A was on average 57 % less than that of R134a for heat fluxes between 30 kWm^{-2} and 110 kWm^{-2}. A model was developed to predict both single-component and multi-component pool boiling of the test refrigerants on the Turbo-ESP surface. The model accounts for viscosity effects on bubble population and uses the Fritz (1935) equation to account for increased vapor production with increasing superheat. Both loss of available superheat and mass transfer resistance effects were modeled for the refrigerant mixtures. For most heat fluxes, the model predicted the measured superheat to within ± 0.31 K.

Keywords: boiling, enhanced heat transfer, refrigerants, structured surface

TABLE OF CONTENTS

LIST OF FIGURES

LIST OF TABLES

INTRODUCTION

As far as heat transfer augmentation is concerned, the use of shell-side boiling enhancements for refrigerants was introduced comparatively late in the history of water-chiller design and manufacture. For example, the commercial application of finned-tubing to enhance the air-side heat transfer performance of products occurred around the time of Wilhelm Maybach's US patent for an augmented automobile radiator (Maybach, 1902). A single-phase, shell-and-tube, heat exchanger with corrugated heat transfer enhancements on both fluid-sides was commercially available by 1921 (Bergles, 1988). The first refrigeration and air-conditioning manufacturers were quick to adopt air-side enhancement for their early products. For example, one of the first companies was established in 1922-1923 to manufacture finned tube heat exchangers for heating and cooling air (Donaldson et al., 1995 and Aerofin, 2017). However, this was not the case for refrigerant-shell-side enhancement. Smooth tubes were exclusively used in air-conditioning and refrigeration chillers up until 1938 (Rogers, 1961). The first commercial shell-side-enhanced, boiling surface for refrigerants was made possible by a joint venture between a tube manufacturer and an air-conditioning manufacturer when they made use of US patent 1,761,733 (Locke, 1930) for making integral-low-finned tubes (Rogers, 1961). In 1938, the value of the extended surface was seen merely as an increase in the heat transfer surface area per unit length.

It wasn't until 1971 that a commercial boiling tube was made specifically for the promotion of reentrant boiling, which was achieved by using a "bent fin" (Kedzierski, 1999). The US patent 3,696,861 (Webb, 1972) for the bent fin was a simple modification of the low-fin tube by raking the fins back upon themselves producing a specified gap between the fin-tip and the adjacent fin for escaping bubbles. Since then, the enhanced boiling tube for refrigerants and process fluids has evolved into significantly more intricate surfaces than the bent-fin. This paper investigates the performance of one of the newer boiling surfaces, i.e., Turbo-ESP[1], with newer refrigerants.

Tests with newer refrigerants are necessary due to pressure from the policies set by the Montreal Protocol (1987) concerning ozone depletion potential (ODP), and the European F-gas Regulation (EU, 2014) and the Kigali amendment to the Montreal Protocol (UNEP, 2016), which regulate the future use of refrigerants with high global warming potential (GWP). These policies have caused a recent shift to refrigerants with both zero ODP and low-GWP. Refrigerant R134a, ubiquitously used for air-conditioning and refrigeration applications, has zero ODP, but a rather large 100-year horizon GWP[2] of 1300 (Myhre et al., 2013). Three new refrigerants, R1234yf (2,3,3,3-Tetrafluoropropene), R513A (R1234yf/R134a (56/44 by mass)), and R450A (R134a/R1234ze (42/58 by mass)), are potential low-GWP replacements for R134a having GWPs of <1 (Myhre et al., 2013), 573, and 547[3], respectively.

---

[1] Certain trade names and company products are mentioned in the text or identified in an illustration in order to adequately specify the experimental procedure and equipment used. In no case does such an identification imply recommendation or endorsement by the National Institute of Standards and Technology, nor does it imply that the products are necessarily the best available for the purpose.

[2] All GWP values are given for zero contribution from climate-carbon feedbacks.

[3] GWP values for R513A and R450A were calculated with a mass fraction weighed sum of the single component values given by Myhre et al. (2013).

The three new refrigerants have zero ODP. The ANSI/ASHRAE Standard 34-(2016) safety classification for R134a, R513A and R450A are A1, indicating that the refrigerants are nonflammable and have low toxicity. The safety classification for R1234yf is A2L, which designates that the refrigerant has a low toxicity and a lower flammability.

Initial work toward the objective of establishing a database for low-GWP refrigerant boiling heat transfer has been present in several recent papers for the new refrigerant R1234yf on non-mechanically-formed-reentrant cavity surfaces. In large part, these investigations show that the boiling performance of R1234yf is comparable to that of R134a. For example, Park and Jung (2010) measured boiling heat transfer coefficients for R1234yf that were similar to those for R134a for a plain and a low-fin surface. In addition, Moreno et al. (2013) showed that the measured pool boiling performance of R1234yf and R134a were nearly identical at lower heat fluxes. However, their measurements for R1234yf yielded lower heat transfer coefficients at higher heat fluxes and a lower critical heat flux (CHF) as compared to R134a. Moreno et al. (2013) also tested a microporous coating with R1234yf and R134a. The coating enhanced both the boiling heat transfer coefficients and CHF for both refrigerants at all tested pressures.

A few boiling investigations for refrigerants have been done for mechanically formed reentrant cavity surfaces that are similar to the structure of the Turbo-ESP surface. Lee et al. (2014) presented boiling heat transfer measurements for R1234yf and R134a on a flat plain, a Turbo-B, a Turbo-C, and a Thermoexcel-E surface. For all tested heat fluxes, their measurements showed that the boiling heat transfer coefficient for each surface was nearly the same for R1234yf and R134a. Gorgy and Eckels (2010) presented measurements of pool boiling of R134a and R123 on Turbo-BII-HP and Turbo-BII-LP tube bundles, respectively, as well as on smooth tube bundles. Gorgy and Eckels (2012) presents experimental investigation of pool boiling on Turbo-BII-HP and Turbo-BII-LP single tubes for R134a and R123, respectively.

The only boiling measurements that were found in the literature for the Turbo-ESP surface were by Gorgy (2016). Gorgy (2016) presents an experimental investigation of the heat transfer performance of R123, R134a, R1234ze, R1233zd(E), and R450A on the Turbo-ESP. The results show that the performance of R1234ze is very similar to that of R134a while R450a shows performance degradation of 28% compared to R134a. The boiling heat transfer for R1233zd(E) was 19% greater than that for R123.

Because of the relatively recent introduction of R1234yf, R513A, and R450A, the availability of measured pool boiling heat transfer data in the literature is limited for these refrigerants. Only a single study for the Turbo-ESP surface (Gorgy, 2016), which did not include the performance of R1234yf and R513A, exists in the literature. Consequently, the present study provides pool boiling heat transfer measurements for R134a, R1234yf, R513A, and R450A on the horizontal, flat, copper, Turbo-ESP-finned surface for test conditions that are applicable for air-conditioning applications.

APPARATUS

Figure 1 shows a schematic of the apparatus that was used to collect the pool boiling. More specifically, the apparatus was used to measure the liquid saturation temperature (T_s), the average pool-boiling heat flux (q''), and the wall temperature (T_w) of the test surface. The

three principal components of the apparatus were a test chamber containing the test surface, the condenser, and the purger. The internal dimensions of the test chamber were 25.4 mm × 257 mm × 1.54 m. The test chamber was charged with approximately 7 kg of refrigerant, giving a liquid height of approximately 80 mm above the test surface. As shown in Fig. 1, the test section was visible through two opposing, flat 150 mm × 200 mm quartz windows. The bottom of the test surface was heated with high velocity (2.5 m/s) water flow. The vapor produced by liquid boiling on the test surface was condensed by the brine-cooled, shell-and-tube condenser and returned as liquid to the pool by gravity. Further details of the test apparatus can be found in Kedzierski (2002) and Kedzierski (2001).

TEST SURFACE

Figure 2 shows the oxygen-free high-conductivity (OFHC) copper flat test plate used in this study. The test plate was machined out of a single piece of OFHC copper by electric discharge machining (EDM). The internal fins of a commercial 25 mm (outer-diameter) Turbo-ESP tube were removed by EDM. The tube was then cut axially, annealed, flattened, and soldered onto the top of the test plate. Figure 3 shows a photograph of the fin surface. The Turbo-ESP has approximately 1968 fins per meter (fpm) oriented along the short axis of the plate. The overall fin-height and the width of the surface openings at the fin-tips are approximately 0.4 mm and 0.04 mm, respectively.

MEASUREMENTS AND UNCERTAINTIES

The standard uncertainty is the positive square root of the estimated variance. The individual standard uncertainties are combined to obtain the expanded uncertainty (U), which is calculated from the law of propagation of uncertainty with a coverage factor. All measurement uncertainties are reported at the 95 % confidence level except where specified otherwise. Further detail on the heat transfer measurement uncertainties can be found in Appendix A.

All of the copper-constantan thermocouples and the data acquisition system were calibrated against a glass-rod standard platinum resistance thermometer (SPRT) and a reference voltage to a residual standard deviation of 0.005 K. Considering the fluctuations in the saturation temperature during the test and the standard uncertainties in the calibration, the expanded uncertainty of the average saturation temperature was no greater than 0.04 K. Consequently, it is estimated that the expanded uncertainty of the temperature measurements was less than 0.1 K.

Twenty 0.5 mm diameter thermocouples were force fitted into the wells of the side of the test plate shown in Fig. 2. The heat flux and the wall temperature were obtained by regressing the measured temperature distribution of the block to the governing two-dimensional conduction equation (Laplace equation). In other words, rather than using the boundary conditions to solve for the interior temperatures, the interior temperatures were used to solve for the boundary conditions following a backward stepwise procedure given in Kedzierski (1995)[4]. As shown in Fig. 2, the origin of the coordinate system was centered on the surface

[4] Table 1 provides functional forms of the Laplace equation that were used in this study in the same way as was done in Kedzierski (1995) and in similar studies by this author.

with respect to the y-direction at the heat transfer surface. Centering the origin in the y-direction reduced the uncertainty of the wall heat flux and temperature calculations by reducing the number of fitted constants involved in these calculations.

Fourier's law and the fitted constants from the Laplace equation were used to calculate the average heat flux (q'') normal to and evaluated at the heat transfer surface based on its projected area. The average wall temperature (T_w) was calculated by integrating the local wall temperature (T). The wall superheat was calculated from T_w and the measured temperature of the saturated liquid (T_s). Considering this, the relative expanded uncertainty in the heat flux ($U_{q''}$) was greatest at the lowest heat fluxes, approaching 12 % of the measurement near 10 kW/m^2. In general, the $U_{q''}$ remained approximately between 3 % and 7 % for heat fluxes greater than 20 kW/m^2. The average random error in the wall superheat (U_{Tw}) remained mainly between 0.06 K and 0.1 K with an average value of approximately 0.085 K. Plots of $U_{q''}$ and U_{Tw} versus heat flux can be found in Appendix A.

EXPERIMENTAL RESULTS

The heat flux was varied between approximately 10 kW/m^2 and 120 kW/m^2 to simulate a range of possible operating conditions for R134a chillers. All pool-boiling measurements were made at 277.6 K saturated conditions. The data were recorded consecutively starting at the largest heat flux and descending in intervals of approximately 4 kW/m^2. The descending heat flux procedure minimized the possibility of any hysteresis effects on the data, which would have made the data sensitive to the initial operating conditions. Table 2 presents the measured heat flux and wall superheat for all the data of this study. Table 3 gives the number of test days and data points for each fluid. A total of 937 measurements were made over 37 days.

Figure 4 is a plot of the measured boiling heat flux (q'') for versus the measured wall superheat ($T_w - T_s = \Delta T_s$) for R134a and R450A on the Turbo-ESP at a saturation temperature of 277.6 K. The open circles and open stars represent the measured data for R134a and R450A, respectively. The solid line is a cubic best-fit regression or estimated mean of the data. Thirteen test days with R134a produced 327 measurements over a period of approximately one month. Twelve of the 327 measurements were removed before fitting because they were statistically identified as “outliers” based on having both high influence and high leverage (Belsley et al., 1980). The data sets for each test fluid presented in this manuscript exhibited a similar number of outliers and were regressed in the same manner. Surface aging data (i.e., “break-in” data) also were not included in the analyzed data sets. The surface aging data typically occurred for each fluid over the first or first and second test days and deviated significantly from the mean of the succeeding and consecutive measurements made over eight to 13 days. Surface aging was not observed over the included data because the between-run variation was approximately random.

Table 4 gives the constants for the cubic regression of the superheat versus the heat flux for all of the fluids tested here. The residual standard deviation of the regressions – representing the proximity of the data to the mean – are given in Table 5 and are, on average, approximately 0.08 K. The dashed lines to either side of the mean represent the lower and upper 95 % simultaneous (multiple-use) confidence intervals for the mean and are, for the

most part, concealed by the data symbols. From the confidence intervals, the expanded uncertainty of the estimated mean wall superheat was, on average, 0.04 K. Table 6 provides the average magnitude of the 95 % multi-use confidence interval for the fitted wall superheat for all of the test data. Table 7 provides selective fluid properties for the test refrigerants evaluated with REFPROP (Lemmon, et al., 2013) at 277.6 K.

Figure 4 compares pool boiling measurements of the present study to those of Gorgy (2016) for R134a and R450A on the Turbo-ESP surface at a saturation temperature of 277.6 K. The Gorgy (2016) measurements are represented by large-dashed gray and black lines for R134a and R450A measurements, respectively. The lines were taken from correlated fits that were provided in Gorgy (2016). The Gorgy (2016) measurements were obtained by means of a Wilson (1915) plot for a test section consisting of three 914 mm long, water cooled tubes in a 245 mm shell. For the same wall superheat, the Gorgy (2016) heat flux for R134a is on average approximately 20 % less than the heat flux measured in the present study for R134a. The maximum deviation occurs at a wall superheat of approximately 1.6 K for R134a where the Gorgy (2016) measurements are approximately 26 % less than the present measured heat fluxes. The best agreement for R134a is for wall superheats between 0.5 K and 1.0 K where the two measurement sets are within ± 10 %. Conversely, the Gorgy (2016) heat fluxes for R450A and the same wall superheat are on average 24 % larger than those measured here for R450A. The best agreement between the two R450A data sets for a range of superheats is between superheats of 1.8 K and 4.2 K where the Gorgy (2016) measurements are within 25 % of the present measurements. The best agreement for a single superheat is for a wall superheat of approximately 2.9 K where the Gorgy (2016) heat flux is only 15 % larger than the mean heat flux measured in the present study. Some of the difference between the present measurements and those of Gorgy (2016) may be attributed to manufacturing tolerances between the two test surfaces; the effect of averaging heat fluxes over different test section lengths; an indirect versus a direct measurement method; and a round tube versus a flat test section. Considering the potential sources for differences, it is believed that the above comparison corroborates the validity of the measurements for R134a and R450A on the Turbo-ESP surface.

Figure 5 compares the pool boiling heat flux (q'') versus the wall superheat (T_w - T_s) for on the Turbo-ESP surface measured in this study for the four test fluids: R134a, R1234yf, R513A, and R450A at a saturation temperature of 277.6 K. Comparison of the mean boiling curves shows that the heat transfer performance of R134a exceeds that of the replacement refrigerants for measured superheats greater than approximately 0.6 K. The boiling curves for R1234yf and R513A are nearly the same being approximately within 4 % of each other and roughly 20 % less than the heat flux for R134a for superheats greater than 1.3 K. By comparison, the heat flux for R450A is roughly 50 % less than that for R134a.

Figure 6 shows a more precise illustration of the relative boiling heat transfer given in Fig. 5. Figure 6 plots the ratio of the heat flux for each replacement refrigerant to that of R134a at the same wall superheat. The heat flux ratio is shown as a solid line with dashed lines and shaded regions representing the 95 % multi-use confidence level for each mean. A heat transfer degradation exists where the heat flux ratio is less than one and the 95 % simultaneous confidence intervals (depicted by the shaded regions) do not include the value

one. The minimum heat flux ratio for R1234yf and R513A was 0.79 ± 0.015, and 0.77 ± 0.03, respectively, which occurred at heat fluxes near 60 kW/m^2. The heat flux ratio for R450A was 0.50 ± 0. 03 at a heat flux of approximately 90 kW/m^2. The average heat flux ratio for R1234yf and R513A was 0.84 and 0.81, respectively, for R134a heat fluxes between 20 kWm^{-2} and 110 kWm^{-2}. The average heat flux ratio for R450A was 0.43 for R134a heat fluxes between 30 kWm^{-2} and 110 kWm^{-2}.

POOL BOILING MODEL

The following describes the development of a model for the pool boiling of the single-component refrigerants and multi-component refrigerant mixtures of this study on the Turbo-ESP surface.

Single Component

The total boiling heat flux is modeled as a sum of the boiling phase-change heat flux (q''_b) and the heat flux due to single phase convection (q''_c):

$$q'' = q''_b + q''_c = n_b \left(h_{fg} \rho_v V_b + \rho_l c_{pl} V_{bL} \Delta T_s \right) \tag{1}$$

where n_b is the number of bubbles generated per unit time and per unit area. In addition, the properties of the refrigerant are the latent heat of vaporization (h_{fg}), the vapor density (ρ_v), the liquid density (ρ_l), and the liquid specific heat (c_{pl}). The average volume of a single bubble is V_b and the volume of superheated liquid that a single bubble carries away with it into the bulk liquid is V_{bL}.

Following the work of Mikic and Rohsenow (1969) who showed that the number of active sites is proportional to the wall superheat raised to some power, the n_b, which is strongly related to the number of active sites, is assumed to be:

$$n_b = c_0 \Delta T_s^m \tag{2}$$

where c_0 is a constant while the exponent m is proposed here to be a function of the probability of a site being active, which is assumed to be directly related to the ratio of the thermal boundary layer thickness (δ) and the bubble diameter (D_b):

$$m = \frac{\delta}{D_b} = c_1 \sqrt{\frac{\mu_l \left(\rho_l - \rho_v \right)}{c_{pl} \cdot \sigma}} \tag{3}$$

Equation (3) was derived by using the approximation for the pool boiling thermal boundary layer thickness proportionality as the square-root of the ratio of the liquid viscosity to the liquid specific heat ($\sqrt{\mu_l / c_{pl}}$) from Kedzierski (2007) and the bubble diameter from Fritz (1935) with all the non-property parameters combined into a single constant c_1. Larger active site densities occur for thicker boundary layers (Hsu, 1962) and for smaller bubbles because the bubbles are less likely to grow beyond the boundary layer and recondense. A larger value for

m represents a greater probability that more sites will be active, which will be reflected in a larger value for n_b.

The Fritz (1935) expression for the bubble diameter is also used to obtain a relation for the volume of a single bubble as:

$$V_b = c_4 D_b^3 = c_3 \left(\frac{\sigma}{(\rho_l - \rho_v)} \right)^{3/2} \tag{4}$$

Here again, all of the fixed constants, including those of the Fritz (1935) equation, were grouped together into a single constant c_3. The constant c_4 makes the relationship between volume and diameter correct and is assimilated into constant c_3.

Substitution of eqs. (2) through (4) into eq. (1), and regression against the measured heat flux and wall superheat for the single component refrigerants R134a and R1234yf yields a pool boiling expression for the two pure refrigerants on the Turbo-EPS surface as:

$$q'' = \Psi h_{fg} \rho_v \left(\frac{\sigma}{(\rho_l - \rho_v)} \right)^{3/2} \Delta T_s^{\beta \sqrt{\frac{\mu_l (\rho_l - \rho_v)}{c_{pl} \cdot \sigma}}} \tag{5}$$

Regression with the measurements showed that the q_c'' term was not statistically significant and was consequently omitted from the model. The leading regression constant of eq. (5), Ψ, is dimensional and equal to 42×10^4 $s^2K^{-1}m^{-7/2}$. Clearly, Ψ is applicable to only the Turbo-EPS surface because it is highly dependent on the number of bubbles generated per unit area per second. It is expected that the regression constant in the exponent, ($\beta = 7.51$ $kg^{-1} \cdot m^2 \cdot K^{-1/2} \cdot W^{1/2}$), would be potentially less surface dependent and more universal for reentrant cavity surfaces. Future work would involve using eq. (5) to regress other reentrant cavity surfaces and other fluids to obtain new regression constants for each boiling surface.

Figure 7 compares eq. (5) to the pool boiling measurements for R134a and R1234yf of the present study. All but ten of the R1234yf measured heat fluxes were predicted to within ± 5 %. For superheats greater than 1.5 K, most of the R134a measured heat fluxes were predicted to within ± 10 %. For superheats less than 1.5 K, the R134a measured heat fluxes were predicted to within ± 10 %. The larger difference between measurements and predictions for the R134a data was due mainly to the larger scatter in the data as compared to that for R1234yf. This is evident in the average difference between measurements and predictions for R134a being 0.7 % implying the data was well centered on the predictions. The superheat for both fluids is predicted to within ± 0.31 K.

Multi-Components

The following section develops a correction multiplier for eq. (5) to make it valid for the multi-component mixtures R513A and R450A. The multiplier is a product of the heat transfer degradation due to the loss of available superheat (Shock, 1982) and that due to mass transfer resistance.

To calculate the boiling heat transfer degradation associated with the loss of available superheat, it was assumed that the difference between the dew-point temperature (T_d) and the bubble-point temperature (T_b), i.e., the temperature glide (ΔT_g), reduces the effective superheat for boiling. In other words, the ΔT_g is not available for boiling and the superheat must exceed ΔT_g before boiling can occur. Following this assumption, the heat transfer degradation due to the loss of available superheat was estimated as:

$$\frac{q_g''}{q''} = \left(1 - \frac{\Delta T_g}{\Delta T_s}\right)^{\beta\sqrt{\frac{\mu_l(\rho_l-\rho_v)}{c_{pl}\cdot\sigma}}} \tag{6}$$

where β is equal to 7.51 $kg^{-1}\cdot m^2\cdot K^{-1/2}\cdot W^{1/2}$.

According to Schlunder (1983), back-diffusion of the higher-boiling component can be modeled by examining the ratio of this diffusion to the vaporization rate. The magnitude of the diffusion is proportional to the temperature glide. The evaporation rate is proportional to the heat flux given by eq. (5). Consequently, the heat transfer degradation due to the mass transfer resistance was estimated as:

$$\frac{q_d''}{q''} = \left(1 - \frac{1.29\Delta T_g}{\Delta T_s^{\beta\sqrt{\frac{\mu_l(\rho_l-\rho_v)}{c_{pl}\cdot\sigma}}}}\right) \tag{7}$$

By using eqs. (6) and (7) as multiplying factors for eq. (5), pool boiling heat flux from the Turbo-ESP surface can be modeled for mixtures (q_m'') as:

$$q_m'' = \Psi h_{fg}\rho_v\left(\frac{\sigma}{(\rho_l-\rho_v)}\right)^{3/2} \Delta T_s^{\beta\sqrt{\frac{\mu_l(\rho_l-\rho_v)}{c_{pl}\cdot\sigma}}} \left(1 - \frac{\Delta T_g}{\Delta T_s}\right)^{\beta\sqrt{\frac{\mu_l(\rho_l-\rho_v)}{c_{pl}\cdot\sigma}}} \left(1 - \frac{1.29\Delta T_g}{\Delta T_s^{\beta\sqrt{\frac{\mu_l(\rho_l-\rho_v)}{c_{pl}\cdot\sigma}}}}\right) \tag{8}$$

The regression constants Ψ and β are the same as those given in eq. (5) and are 42 $\times 10^4$ $s^2K^{-1}m^{-7/2}$ and 7.51 $kg^{-1}\cdot m^2\cdot K^{-1/2}\cdot W^{1/2}$, respectively.

Figure 8 compares eq. (8) to the pool boiling measurements for R513A and R450A of the present study. For heat fluxes between 10 kWm^{-2} and 80 kWm^{-2}, the superheats for both fluids are predicted to within ± 0.3 K. On average, the heat flux is predicted to within ± 14 % and ± 4 % for R513A and R450A, respectively. Larger percent deviations in the heat flux occur for the lowest and highest test heat fluxes.

CONCLUSIONS

The pool boiling performance of a R134a, R1234yf, R513A, and R450A on a flattened, horizontal Turbo-ESP surface was investigated. The study showed that the boiling performance of R134a on the Turbo-ESP exceeded that of the replacement refrigerants for heat fluxes greater than 20 kWm^{-2}. On average, the heat flux for R1234yf and R513A were 16 % and 19 % less than that for R134a, respectively, for R134a heat fluxes between 20 kWm^{-2} and 110 kWm^{-2}. The heat flux for R450A was on average 57 % less than that of R134a for heat fluxes between 30 kWm^{-2} and 110 kWm^{-2}.

A model was developed to predict both single-component and multi-component pool boiling of the test refrigerants on the Turbo-ESP surface. The model accounts for viscosity effects on bubble population and uses the Fritz (1935) equation to account for increased vapor production with increasing superheat. Both loss of available superheat and mass transfer resistance effects were modeled for the refrigerant mixtures. For most heat fluxes, the model predicted the measured superheat to within ± 0.31 K.

ACKNOWLEDGEMENTS

This work was funded by the National Institute of Standards and Technology (NIST). Thanks go to D. Han of Ingersoll Rand and to the following NIST personnel for their constructive criticism of the draft manuscript: D. Veronica and P. Domanski. Furthermore, the author extends appreciation to W. Guthrie and A. Heckert of the NIST Statistical Engineering Division for their consultations on the uncertainty analysis. In-kind donations of the test refrigerants by K. Kontomaris of Chemours and S. Yana Motta of Honeywell are greatly appreciated.

NOMENCLATURE

English Symbols

A_n	regression constant in Table 4 n=0,1,2,3
c_n	regression constants in eqs. (2) through (4) n=0,1,2,3,4
c_{pl}	specific heat of liquid, J kg^{-1} K^{-1}
D_b	bubble diameter, m
h_{fg}	latent heat of vaporization, J kg^{-1}
k	thermal conductivity, $W \cdot m^{-1} \cdot K^{-1}$
L	test surface length shown in Fig. 3, m
m	exponent term in eq. (2) and defined in eq. (3)
n_b	number of bubbles per unit time per unit area, $s^{-1}m^{-2}$
P	pressure, Pa
q"	average wall heat flux based on projected area, $W \cdot m^{-2}$
T	temperature, K
u	velocity, $m \cdot s^{-1}$
U	expanded uncertainty
V	volume, m^3
X	model terms given in Table 1

Greek symbols

β	dimensional constant in eqs. (5) through (8), 7.51 $kg^{-1} \cdot m^2 \cdot K^{-1/2} \cdot W^{1/2}$
δ	thermal boundary layer thickness, m
ΔT_g	temperature glide: T_d - T_b, K
ΔT_s	wall superheat: T_w - T_s, K
μ	dynamic viscosity, $kg \cdot m^{-1} \cdot s^{-1}$
σ	surface tension of refrigerant, $N \cdot m^{-1}$
ρ	density, $kg \cdot m^{-3}$
Ψ	dimensional constant in eqs. (5) and (8), 42 $\times 10^4$ $s^2K^{-1}m^{-7/2}$

English Subscripts

d	diffusion or dew point
b	bubble or bubble point
bL	bubble layer
c	convection
g	glide
l	liquid refrigerant
m	mixture
q"	heat flux
s	saturated state, streaming
w	wall temperature
v	refrigerant vapor

REFERENCES

Aerofin. 2017. http://www.aerofin.com/about/history.

ASHRAE. 2016. Designation and Safety Classification of Refrigerants, ANSI/ASHRAE Standard 34-2016.

Belsley, D. A., Kuh, E., and Welsch, R. E. 1980 Regression Diagnostics: Identifying Influential Data and Sources of Collinearity, New York: Wiley.

Bergles, A. E. 1988. Enhancement of Convective Heat Transfer Newton's Legacy Pursued, Presented at 25th Natl. Heal Transfer conf., Houston, TX, August 1988; History of Heat Transfer, ASME, New York, pp. 53-64.

Donaldson, B., Nagengast, B., and Meckler, G. 1995. Heat and Cold: Mastering the Great Indoors: A Selective History, ASHRAE, New York, p. 261.

EU. 2014. Regulation (Eu) No 517/2014 of the European Parliament and of the Council of 16 April 2014 on fluorinated greenhouse gases and repealing Regulation (EC) No 842/2006, Official Journal of the European Union, L 150/195, http://data.europa.eu/eli/reg/2014/517/oj.

Fritz, W. 1935. Berechnung des Maximalvolume von Dampfblasen, Physikalische Zeitschrift, 36, 379-388.

Gorgy, E. 2016. Nucleate boiling of low-GWP refrigerants on highly enhanced tube surface, Int. J. Heat Mass Transfer, 96, 660–6.

Gorgy, E, and Eckels, S. 2012. Local heat transfer coefficient for pool boiling of R-134a and R-123 on smooth and enhanced tubes. Int. J. Heat Mass Transfer, 55, 3021–8.

Gorgy, E., and Eckels, S. 2010. Average Heat Transfer Coefficient for Pool Boiling of R-134a and R-123 on Smooth and Enhanced Tubes (RP-1316). HVAC&R Res, 16, 657–76.

Hsu, Y. Y. 1962. On the Size Range of Active Nucleation Cavities on a Heating Surface, J. Heat Transfer, 84, 207-216.

Kedzierski, M. A. 2007. Effect of Refrigerant Oil Additive on R134a and R123 Boiling Heat Transfer Performance, Int. J. Refrigeration, 30(1), 144-154.

Kedzierski, M. A. 2002. Use of Fluorescence to Measure the Lubricant Excess Surface Density During Pool Boiling, Int. J. Refrigeration, 25, 1110-1122.

Kedzierski, M. A. 2001. Use of Fluorescence to Measure the Lubricant Excess Surface Density During Pool Boiling, NISTIR 6727, U.S. Department of Commerce, Washington, D.C.

Kedzierski, M. A. 1999. Ralph L. Webb: A Pioneering Proselytizer for Enhanced Heat Transfer, J. Enhanced Heat Transfer, 6(2-4), 71-78.

Kedzierski, M. A. 1995. Calorimetric and Visual Measurements of R123 Pool Boiling on Four Enhanced Surfaces, NISTIR 5732, U.S. Department of Commerce, Washington.

Lee, Y., Kang, D. G., Kim, J. H., Jung, D. 2014. Nucleate boiling heat transfer coefficients of HFO1234yf on various enhanced surfaces. Int. J. Refrigeration, 38, 198–205.

Lemmon, E. W., Huber, M. L., and McLinden, M. O. 2013. *NIST Standard Reference Database 23 (REFPROP), Version 9.1*., National Institute of Standards and Technology, Boulder, CO.

Locke, A., A. 1930. Integral Finned Tubing and Method of Manufacturing the Same, US Patent 1,761,733.

Maybach, W. 1902. Cooling and condensing apparatus, US patent 709416 A.

Mikic, B., B, and Rohsenow, W. M. 1969. A New Correlation of Pool-Boiling Data Including the Effect of Heating Surface Characteristics, J. Heat Transfer, 91(2), 245-250.

Moreno, G., Narumanchi, S., King, C. 2013. Pool Boiling Heat Transfer Characteristics of HFO-1234yf on Plain and Microporous-Enhanced Surfaces, J. Heat Transfer, 135, 111014.

Montreal Protocol 1987. *Montreal Protocol on Substances that Deplete the Ozone Layer*. United Nations (UN), New York, NY, USA (1987 with subsequent amendments).

Myhre, G., D. Shindell, F.-M. Bréon, W. Collins, J. Fuglestvedt, J. Huang, D. Koch, J.-F. Lamarque, D. Lee, B. Mendoza, T. Nakajima, A. Robock, G. Stephens, T. Takemura and H. Zhang. 2013. Anthropogenic and Natural Radiative Forcing Supplementary Material. In: *Climate Change 2013: The Physical Science Basis. Contribution of Working Group I to the Fifth Assessment Report of the Intergovernmental Panel on Climate Change* [Stocker, T.F., D. Qin, G.-K. Plattner, M. Tignor, S.K. Allen, J. Boschung, A. Nauels, Y. Xia, V. Bex and P.M. Midgley (eds.)]. Available from www.climatechange2013.org and www.ipcc.ch.

Park, K. J., Jung, D. 2010. Nucleate boiling heat transfer coefficients of R1234yf on plain and low fin surfaces. Int. J. Refrigeration, 33, 553–7.

Rogers, J. S. 1961. Study of Low-Fin Tube 1929-1960, Wolverine Tube, Inc, Internal Report Neshan-1, p. 8.

Schluender, E. U. 1983. Heat transfer in nucleate boiling of mixtures. Int. Chemical Engineering, 23(4), 589-599.

Shock, R. A. W. 1982. Boiling in Multicomponent Fluids, Multiphase Science and Technology, Hemisphere Publishing Corp, 1, 281-386.

UNEP, 2016. Amendment to the Montreal Protocol on Substances that Deplete the Ozone Layer, Kigali, 15 October 2016. https://treaties.un.org/doc/Publication/CN/2016/CN.872.2016-Eng.pdf (accessed July 25, 2017).

Webb, R. L. 1972. Heat Transfer Surface Having a High Boiling Heat Transfer Coefficient, US patent 3,696,861.

Wilson, E.E. 1915. A Basis for Rational Design of Heat Transfer Apparatus, Trans. ASME, 37, 47-70.

Table 1 Conduction model choice

X_0= constant (all models) X_1= x X_2= y X_3= xy $X_4=x^2-y^2$ $X_5= y(3x^2-y^2)$ $X_6= x(3y^2-x^2)$ $X_7= x^4+y^4-6(x^2)y^2$ $X_8= yx^3-xy^3$	
Fluid	Most frequent models
R134a 0.6 K ≤ ΔT_s ≤ 3.0 K	X_1,X_3 (131 of 315) 41 % X_1,X_3,X_7 (118 of 315) 37 % X_1,X_3,X_7 ,X_8 (58 of 315) 18 %
R1234yf 0.5 K ≤ ΔT_s ≤ 3.6 K	X_1,X_3 (62 of 198) 31 % X_1,X_2,X_3 (60 of 198) 30 % X_1,X_2,X_3,X_7 (37 of 198) 19 % X_1,X_3,X_7 (35 of 198) 18 %
R513A 0.5 K ≤ ΔT_s ≤ 4.2 K	X_1,X_3 (92 of 194) 48 % X_1,X_3,X_7 (47 of 194) 25 % X_1,X_2,X_3,X_7 (21 of 194) 11 % X_1,X_3,X_7 ,X_8 (20 of 194) 10 %
R450A 0.9 K ≤ ΔT_s ≤ 4.8 K	X_1,X_3 (81 of 196) 41 % X_1,X_3,X_8 (48 of 196) 25 % X_1,X_3,X_7 (32 of 196) 16 % X_1,X_3,X_7 ,X_8 (17 of 196) 9 %

Table 2 Pool boiling data

R134a
File: EPS134a.dat

ΔT_s (K)	q'' (W/m^2)
3.02	109104.
3.02	109108.
3.02	109125.
2.80	102785.
2.80	102749.
2.79	102620.
2.60	96918.
2.60	96930.
2.60	96955.
2.42	91280.
2.43	91360.
2.44	91427.
2.26	85218.
2.27	85256.
2.27	85248.
2.04	75965.
2.05	75967.
2.06	75955.
1.81	67275.
1.81	67330.
1.83	67323.
1.60	58940.
1.60	58898.
1.61	58897.
1.41	50998.
1.42	51202.
1.42	51209.
1.27	42739.
1.29	42624.
1.31	42595.
1.17	35006.
1.18	34959.
1.19	34925.
0.99	28053.
0.99	28073.
1.00	28076.
0.82	22170.
0.84	22091.
0.84	22025.
0.61	16385.
0.61	16371.
2.95	108832.
2.94	108795.
2.94	108905.
2.66	99901.
2.67	99908.
2.66	100033.
2.43	90919.
2.42	90885.
2.42	90992.
2.17	81392.
2.18	81599.
2.19	81724.
1.95	72603.
1.95	72640.
1.95	72531.
1.73	64129.
1.73	64047.
1.73	64047.
1.54	56347.
1.53	56028.
1.53	55916.
1.36	48226.
1.37	48158.
1.39	48111.
1.28	39947.
1.29	39876.
1.30	39789.
1.12	32694.
1.13	32632.
1.13	32580.
0.94	25769.
0.94	25729.
0.95	25710.
0.76	19992.
0.76	19975.
0.77	19982.
0.54	14423.
0.55	14319.
2.95	108192.
2.94	108220.
2.93	108207.
2.67	99551.
2.67	99623.
2.66	99724.
2.41	90598.
2.41	90563.
2.40	90673.
2.16	81574.
2.16	81625.
2.17	81521.
1.92	72070.
1.92	72040.
1.91	72038.
1.69	63903.
1.69	63885.
1.69	63813.
1.49	55979.
1.50	55906.
1.50	56086.
1.30	48521.
1.33	48435.
1.33	48398.
1.18	40293.
1.22	40144.
1.23	40134.
1.10	32665.
1.11	32540.
1.10	32512.
0.93	25946.
0.93	25937.
0.94	25937.
0.72	19701.
0.73	19698.
0.74	19662.
0.51	14234.
0.51	14234.
2.93	107600.
2.93	107673.
2.92	107645.
2.67	99229.
2.67	99243.
2.67	99392.
2.41	90332.
2.42	90411.
2.41	90394.
2.16	81218.
2.17	81119.
2.17	81004.
1.91	71946.
1.91	71877.
1.91	71912.
1.69	63605.
1.69	63450.
1.69	63604.
1.49	55792.
1.49	55764.
1.49	55802.
1.34	48185.
1.35	48112.
1.35	48165.
1.24	39831.
1.25	39773.
1.27	39636.
1.11	32546.
1.11	32497.
1.11	32491.
0.95	26193.
0.96	26141.
0.95	26064.
0.73	20004.
0.73	20009.
0.74	19938.
0.53	14265.
0.52	14295.
2.66	107669.
2.67	107700.
2.66	107732.
2.19	90025.
2.20	89970.
2.20	89953.
1.75	72285.
1.75	72267.
1.75	72283.
1.35	55911.
1.34	55920.
1.34	55875.
1.12	47706.
1.13	47733.
1.13	47703.
0.96	40241.
0.96	40236.
0.97	40199.
0.78	26075.
0.78	26020.
0.78	25986.
0.36	14231.
0.37	14168.
3.14	106209.
3.13	106220.
2.57	89872.
2.56	89889.

1.99	71701.
1.99	71629.
1.45	55555.
1.47	55515.
1.24	48144.
1.24	48336.
1.08	40390.
1.08	40294.
0.99	33018.
0.99	32523.
0.80	26277.
0.81	26279.
0.35	14317.
2.95	108003.
2.95	108026.
2.40	90687.
2.41	90750.
1.92	72607.
1.91	72565.
1.45	56349.
1.47	56272.
1.30	49154.
1.31	49145.
1.13	41332.
1.14	41160.
1.00	33432.
1.00	33456.
0.82	26386.
0.82	26315.
0.35	14895.
2.87	108444.
2.87	108521.
2.33	90667.
2.33	90650.
1.85	72978.
1.84	73044.
1.41	56787.
1.42	56742.
1.23	49159.
1.24	49090.
1.10	40060.
1.09	40066.
0.94	33096.
0.95	33099.
0.79	26146.
0.78	26174.
0.36	14735.
2.88	108653.
2.88	108655.

2.40	91085.
2.40	91047.
1.88	72708.
1.88	72679.
1.44	56114.
1.43	56096.
1.26	48710.
1.27	48675.
1.10	40750.
1.11	40649.
0.95	32793.
0.97	32637.
0.77	25911.
0.79	26366.
0.37	14785.
2.87	108862.
2.87	108951.
2.34	90232.
2.34	90306.
1.84	72723.
1.84	72835.
1.46	56724.
1.46	56590.
1.26	48683.
1.28	48676.
1.13	40258.
1.14	40188.
0.99	33115.
0.99	33117.
0.83	26415.
0.82	26313.
0.39	14384.
2.86	108668.
2.86	108664.
2.86	108801.
2.60	100114.
2.61	100185.
2.61	100210.
2.34	90566.
2.34	90652.
2.34	90650.
2.06	81278.
2.07	81281.
2.07	81329.
1.82	73067.
1.82	73107.
1.81	73117.
1.61	65153.
1.60	65095.

1.60	65065.
1.41	56979.
1.42	56893.
1.42	56811.
1.24	49359.
1.26	49274.
1.27	49141.
1.15	40721.
1.15	40645.
1.14	40619.
0.96	33211.
0.98	33098.
0.97	33005.
0.82	26279.
0.81	26198.
0.80	26169.
0.63	20106.
0.63	20032.
0.63	19980.
0.35	14327.
0.35	14381.
3.04	102998.
3.04	102936.
3.03	102949.
2.69	94058.
2.69	94183.
2.69	94192.
2.38	85509.
2.38	85456.
2.38	85430.
2.05	76494.
1.75	68321.
1.52	60602.
1.29	52809.
1.07	44999.
0.98	36783.
0.82	29793.
2.58	103892.
2.32	95108.
2.07	86372.
1.86	77197.
1.61	68476.
1.36	60731.
1.26	52659.
1.15	43678.
0.96	35906.
0.79	29361.
0.66	23444.

R1234yf
File: EPSyf.dat

ΔT_s (K)	q'' (W/m^2)
3.13	105034.
3.31	102248.
2.94	98428.
2.93	98416.
2.67	89572.
2.66	89530.
2.41	80745.
2.43	80548.
2.21	71752.
2.21	71758.
2.02	63952.
2.03	64197.
1.77	56340.
1.77	56406.
1.52	48612.
1.54	48560.
1.35	41812.
1.35	41752.
1.09	33503.
1.10	33500.
0.87	26848.
0.88	26817.
0.68	20585.
0.68	20510.
0.48	14853.
3.43	106135.
3.43	106096.
3.09	97549.
3.09	97549.
2.78	88813.
2.78	88833.
2.49	80547.
2.50	80537.
2.25	72125.
2.27	72233.
2.06	64274.
2.07	64223.
1.83	56473.
1.83	56331.
1.60	48440.
1.59	48461.
1.37	41049.
1.38	41002.
1.13	32891.
1.14	32844.
0.92	26584.
0.92	26630.
0.72	20214.
0.72	20167.
0.51	14670.
3.53	112532.
3.53	112535.
3.22	103675.
3.20	103676.
2.91	94223.
2.91	94140.
2.65	83963.
2.66	83975.
2.41	75179.
2.42	75126.
2.15	67228.
2.15	67255.
1.90	59563.
1.91	59573.
1.71	51758.
1.72	51334.
1.41	43105.
1.40	42955.
1.17	35948.
1.17	35847.
0.97	28807.
0.96	28739.
0.73	21752.
0.74	21704.
0.49	15348.
3.56	113307.
3.56	113327.
3.33	103935.
3.34	103828.
3.06	93762.
3.06	93768.
2.77	84287.
2.77	84329.
2.47	75596.
2.48	75596.
2.20	67558.
2.18	67344.
1.97	59245.
1.97	59228.
1.70	50938.
1.70	50850.
1.44	43186.
1.44	43176.
1.21	35975.
1.22	35980.
1.00	28917.
0.99	28892.
0.75	21773.
0.75	21679.
0.48	15124.
3.59	112577.
3.59	112547.
3.31	104489.
3.32	104453.
3.04	94315.
3.04	94385.
2.76	84862.
2.76	84772.
2.48	75817.
2.48	75775.
2.20	67384.
2.20	67327.
1.98	59546.
1.98	59567.
1.72	51097.
1.72	51110.
1.46	43514.
1.45	43289.
1.22	36091.
1.22	36037.
0.99	28960.
0.99	28961.
0.77	21954.
0.77	21891.
0.51	15497.
3.53	114222.
3.53	114188.
3.27	105042.
3.28	105089.
3.02	95096.
3.02	95081.
2.73	85382.
2.74	85410.
2.44	76333.
2.44	76424.
2.18	68215.
2.18	68211.
1.95	60197.
1.95	60162.
1.68	51019.
1.67	50934.
1.41	43279.
1.42	43324.
1.18	35907.
1.19	35863.
0.98	28702.
0.97	28589.
0.73	21508.
0.73	21429.
0.51	15390.
3.60	113960.
3.60	114055.
3.31	105737.
3.32	105716.
3.06	96232.
3.06	96208.
2.76	86402.
2.77	86529.
2.48	77631.
2.49	77717.
2.23	69131.
2.23	69202.
2.00	61442.
2.00	61427.
1.75	52629.
1.75	52567.
1.48	44579.
1.48	44556.
1.24	37046.
1.24	37006.
1.01	30227.
1.02	30187.
0.79	23219.
0.79	23184.
0.55	16291.
3.64	114482.
3.64	114557.
3.35	105987.
3.34	105994.
3.08	96376.
3.07	96394.
2.79	86728.
2.79	86619.
2.49	78048.
2.50	78083.
2.25	70099.
2.26	70087.
2.02	61600.
2.02	61431.
1.72	52660.
1.73	52672.
1.47	44951.
1.46	44889.
1.23	37369.

1.25	37614.
1.03	30033.
1.03	30027.
0.80	23219.
0.79	23118.
0.53	16364.
0.54	16277.

R513A
File: EPSXP10.dat

ΔT_s (K)	q'' (W/m^2)
3.92	107920.
3.94	108135.
3.38	104518.
3.37	104348.
3.05	96180.
3.05	96130.
2.71	86652.
2.71	86760.
2.40	77780.
2.40	77791.
2.11	69242.
2.10	69309.
1.86	61431.
1.86	61510.
1.70	53602.
1.71	53597.
1.49	45463.
1.49	45451.
1.27	37277.
1.27	37240.
1.02	29694.
1.02	29688.
0.77	22730.
0.78	22795.
0.49	15831.
4.14	108100.
3.95	113509.
3.54	104872.
3.52	104737.
3.16	95998.
3.16	96044.
2.83	86965.
2.82	86620.
2.48	77486.
2.47	77525.
2.19	69342.
2.19	69412.
1.98	61324.
1.97	61267.
1.76	53107.
1.76	53029.
1.56	45059.
1.54	45044.
1.29	36874.
1.29	36812.
1.03	29476.
1.04	29495.
0.78	22859.
0.78	22863.
0.52	16194.
3.87	113290.
3.86	113475.
3.52	104333.
3.51	104181.
3.16	95535.
3.15	95560.
2.82	86456.
2.80	86246.
2.49	77184.
2.49	77227.
2.25	69374.
2.25	69389.
2.01	61346.
2.01	61323.
1.79	53196.
1.79	53186.
1.54	44625.
1.54	44587.
1.34	36792.
1.33	36762.
1.07	29140.
1.06	29148.
0.81	22460.
0.80	22407.
0.54	16024.
3.81	113412.
3.81	113555.
3.47	105203.
3.47	105300.
3.13	96376.
3.14	96377.
2.80	87255.
2.78	87114.
2.48	78732.
2.49	78887.
2.25	69864.
2.26	69972.
2.03	61229.
2.02	61182.
1.80	53089.
1.79	52958.
1.52	44611.
1.53	44571.
1.28	36868.
1.28	36849.
1.02	29029.
1.02	28992.
0.76	22051.
0.76	22096.
0.49	15626.
3.98	113758.
3.97	113874.
3.64	105500.
3.62	105399.
3.24	96227.
3.24	96187.
2.88	87303.
2.87	87415.
2.56	78563.
2.56	78548.
2.39	70232.
2.38	70189.
2.09	61173.
2.09	61255.
1.84	53258.
1.84	53327.
1.61	45253.
1.60	44861.
1.32	36956.
1.32	36931.
1.06	29205.
1.06	29222.
0.81	22324.
0.80	22234.
0.51	15418.
4.20	113885.
4.20	113677.
3.82	104995.
3.81	105063.
3.45	96826.
3.44	97063.
3.05	87350.
3.07	88140.
2.72	78612.
2.72	78800.
2.41	69590.
2.42	69673.
2.18	61394.
2.17	61426.
1.92	53305.
1.92	53298.
1.64	45160.
1.64	45138.
1.34	37014.
1.34	37072.
1.07	29431.
1.08	29402.
0.80	22281.
0.81	22281.
0.53	15903.
4.13	115525.
4.14	115657.
3.76	106904.
3.76	107173.
3.43	98371.
3.41	98567.
3.01	88305.
3.00	88685.
2.76	80242.
2.75	80269.
2.47	71322.
2.47	71502.
2.18	61696.
2.18	61711.
1.90	53256.
1.90	53160.

1.63	44832.
1.64	44808.
1.34	36450.
1.34	36368.
1.07	28916.
1.07	28980.
0.79	21837.
0.79	21802.
0.49	15062.
3.88	115538.
3.86	115584.
3.47	105737.
3.46	105786.
3.07	96204.
3.06	96206.
2.69	87418.
2.68	87537.
2.35	78194.
2.35	78239.
2.04	69610.
2.04	69313.
1.76	60198.
1.75	60240.
1.51	52532.
1.51	52555.
1.34	45162.
1.36	45097.
1.24	37231.
1.24	37302.
1.04	30086.
1.03	30032.
0.80	23176.
0.79	23209.
0.56	16699.
0.57	16817.

R450A
File: EPSN13.dat

ΔT_s (K)	q'' (W/m^2)
4.56	109453.
4.56	109424.
4.19	99792.
4.19	99805.
3.86	91197.
3.87	91207.
3.56	82538.
3.54	82441.
3.25	74051.
3.25	74076.
2.94	65962.
2.94	66002.
2.65	58130.
2.67	58095.
2.39	50245.
2.39	50249.
2.17	42881.
2.17	42856.
1.97	35519.
1.98	35518.
1.76	28746.
1.74	28701.
1.45	22180.
1.44	22176.
1.12	15827.
1.13	15800.
0.81	9821.
4.52	108668.
4.52	108532.
4.20	100416.
4.19	100491.
3.82	91913.
3.81	91695.
3.54	83258.
3.52	83297.
3.25	75249.
3.25	74939.
2.95	66167.
2.94	66103.
2.68	58083.
2.69	58025.
2.42	50009.
2.41	49939.
2.18	42875.
2.19	42975.
2.03	35927.
2.02	35909.
1.82	29082.
1.82	29029.
1.55	22381.
1.54	22367.
1.14	14998.
1.15	14994.
0.89	9621.
4.89	106521.
4.89	106523.
4.53	97767.
4.10	90005.
4.11	90039.

4.11	90039.
3.76	81248.
4.12	90047.
3.40	72939.
3.38	73031.
3.09	65213.
3.10	65286.
2.78	57421.
2.79	57409.
2.50	49190.
2.50	49224.
2.26	42069.
2.25	42012.
2.04	35226.
2.04	35216.
1.84	28241.
1.81	28254.
1.50	21615.
1.50	21635.
1.17	15145.
1.14	15095.
0.84	9702.
4.58	108857.
4.57	108689.
4.28	99670.
4.26	99720.
3.95	91033.
3.95	91099.
3.67	82622.
3.65	82608.
3.33	74019.
3.34	73982.
3.04	65512.
3.02	65467.
2.75	57303.
2.74	57293.
2.52	49859.
2.52	49813.
2.30	43191.
2.30	43200.
2.07	36109.
2.06	36044.
1.84	28766.
1.82	28799.
1.53	22249.
1.52	22282.
1.19	16012.
1.17	15960.
0.84	9951.
4.86	107955.
4.87	107968.
4.46	99000.
4.46	99033.
4.11	90786.
4.11	90804.
3.78	82467.
3.77	82602.
3.46	74449.
3.46	74496.
3.15	66074.
3.15	66044.
2.85	58203.
2.84	58075.
2.51	49263.
2.52	49495.

2.32	41866.
2.31	41668.
2.07	35162.
2.07	35223.
1.89	29274.
1.87	29280.
1.61	22510.
1.59	22605.
1.30	16055.
1.30	15932.
0.94	9911.
4.57	108452.
4.55	108419.
4.27	99546.
4.24	99648.
3.92	90923.
3.93	90888.
3.64	82397.
3.64	82730.
3.31	74220.
3.32	74137.
3.05	66277.
3.05	66277.
2.73	58678.
2.71	58671.
2.44	50385.
2.44	50375.
2.18	43447.
2.19	43771.
2.05	36472.

2.03	36481.
1.82	29051.
4.84	108265.
4.85	108275.
4.53	98356.
4.53	98327.
4.16	89798.
4.14	89846.
3.82	81768.
3.79	81779.
3.43	73227.
3.42	73273.
3.12	65681.
3.12	65662.
2.83	57560.
2.82	57589.
2.59	50200.
2.55	49871.
2.38	43083.
2.37	42997.
2.21	35577.
2.22	35578.
1.98	28678.
1.97	28658.
1.60	21400.
1.60	21441.
1.30	15207.
1.29	15264.
0.90	9046.
4.74	108629.

4.73	108701.
4.39	99395.
4.39	99439.
4.06	90315.
4.03	90342.
3.77	82038.
3.77	82059.
3.43	73912.
3.41	73845.
3.12	65666.
3.12	65612.
2.86	57350.
2.84	57298.
2.59	49786.
2.59	49788.
2.35	42634.
2.35	43024.
2.16	36036.
2.16	36067.
1.91	28459.
1.90	28488.
1.59	21541.
1.59	21510.
1.35	15451.
1.33	15550.
0.92	8982.
0.93	9010.

Table 3 Number of test days and data points

Fluid (% mass fraction)	Number of days	Number of data points/ Number of data points with outliers removed
R134a $0.6\ \text{K} \le \Delta T_s \le 3.0\ \text{K}$	13	327/315
R1234yf $0.5\ \text{K} \le \Delta T_s \le 3.6\ \text{K}$	8	200/198
R513A $0.5\ \text{K} \le \Delta T_s \le 4.2\ \text{K}$	8	200/194
R450A $0.9\ \text{K} \le \Delta T_s \le 4.8\ \text{K}$	8	210/196

Table 4 Estimated parameters for cubic boiling curve fits for Turbo-ESP copper surface

$\Delta T_s = A_0 + A_1 q'' + A_2 q''^2 + A_3 q''^3$

ΔT_s in kelvin and q'' in W/m^2

Fluid	A_o	A_1	A_2	A_3
R134a 0.6 K ≤ ΔT_s ≤ 3.0 K	0.338869	1.92286×10^{-5}	-5.32439×10^{-12}	4.72520×10^{-16}
R1234yf 0.5 K ≤ ΔT_s ≤ 3.6 K	-0.0482707	3.85174×10^{-5}	-1.23198×10^{-10}	5.83771×10^{-16}
R513A 0.5 K ≤ ΔT_s ≤ 4.2 K	-0.219981	5.35387×10^{-5}	-4.37364×10^{-10}	2.58871×10^{-15}
R450A 0.9 K ≤ ΔT_s ≤ 4.8 K	0.491691	5.38584×10^{-5}	-3.68255×10^{-10}	2.19245×10^{-15}

Table 5 Residual standard deviation of ΔT_s

Fluid	(K)
R134a 0.6 K ≤ ΔT_s ≤ 3.0 K	0.09
R1234yf 0.5 K ≤ ΔT_s ≤ 3.6 K	0.04
R513A 0.5 K ≤ ΔT_s ≤ 4.2 K	0.10
R450A 0.9 K ≤ ΔT_s ≤ 4.8 K	0.10

Table 6 Average magnitude of 95 % multi-use confidence interval for mean ΔT_s

Fluid	U (K)
R134a 0.6 K ≤ ΔT_s ≤ 3.0 K	0.03
R1234yf 0.5 K ≤ ΔT_s ≤ 3.6 K	0.02
R513A 0.5 K ≤ ΔT_s ≤ 4.2 K	0.05
R450A 0.9 K ≤ ΔT_s ≤ 4.8 K	0.05

Table 7 Selective fluid properties of test refrigerants at 277.6 K (Lemmon et al., 2013)

Fluid	P_v (kPa)	ΔT_g (K)	k_l ($mWm^{-1}k^{-1}$)	μ_l ($\mu kg \cdot m^{-1} \cdot s^{-1}$)	σ ($N \cdot m^{-1}$)	ρ_l ($kg\ m^{-3}$)	ρ_v ($kg\ m^{-3}$)	h_{fg} ($kJ\ kg^{-1}$)	c_{pl} ($kJ\ kg^{-1}\ K^{-1}$)
R134a	343.02	0	90.048	251.86	0.010806	1279.9	16.8	195.17	1.3536
R1234yf	366.29	0	70.012	197.31	0.008849	1162.2	20.383	160.39	1.3059
R513A	375.34	0.1	80.692	226.71	0.0099456	1237.8	19.861	172.92	1.3251
R450A	303.98	0.67	84.322	249.45	0.011446	1244.5	15.370	185.62	1.3392

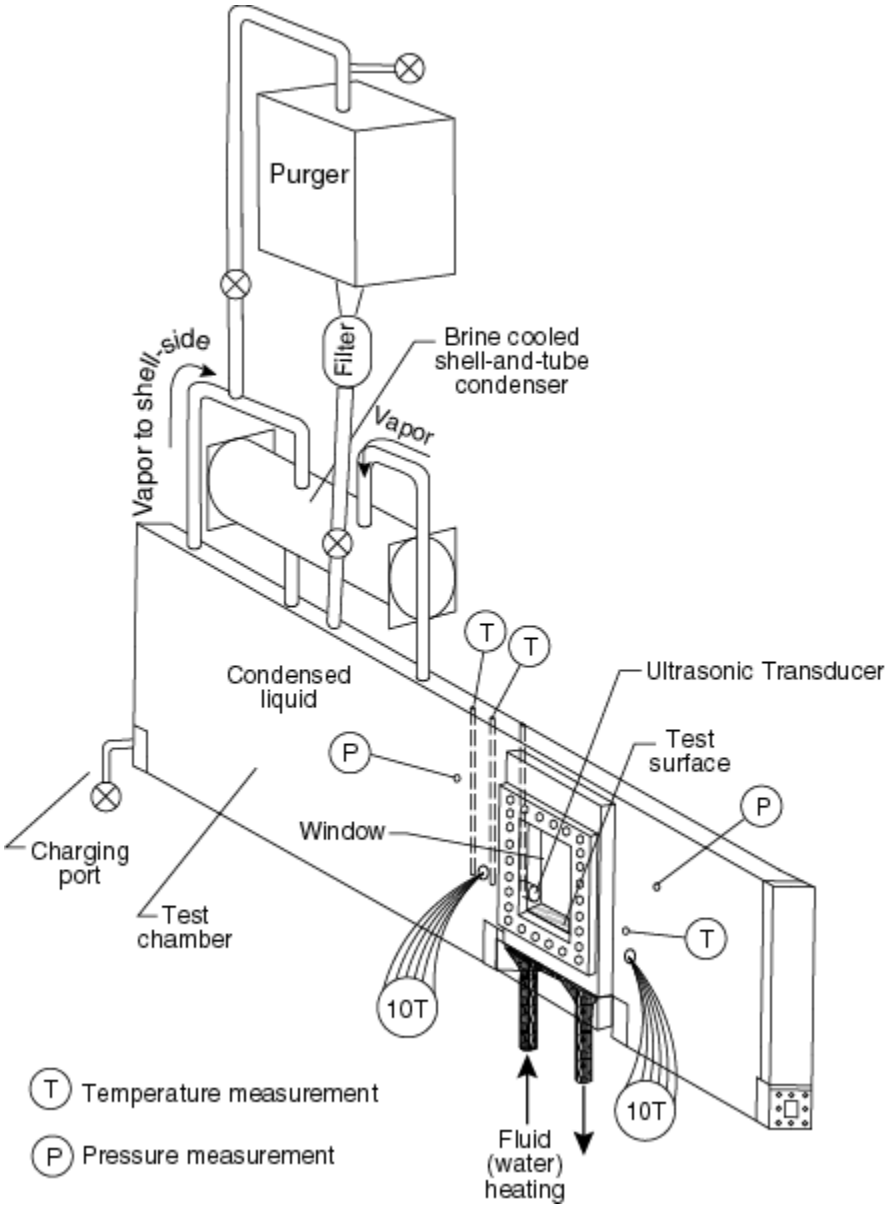

Fig. 1 Schematic of test apparatus

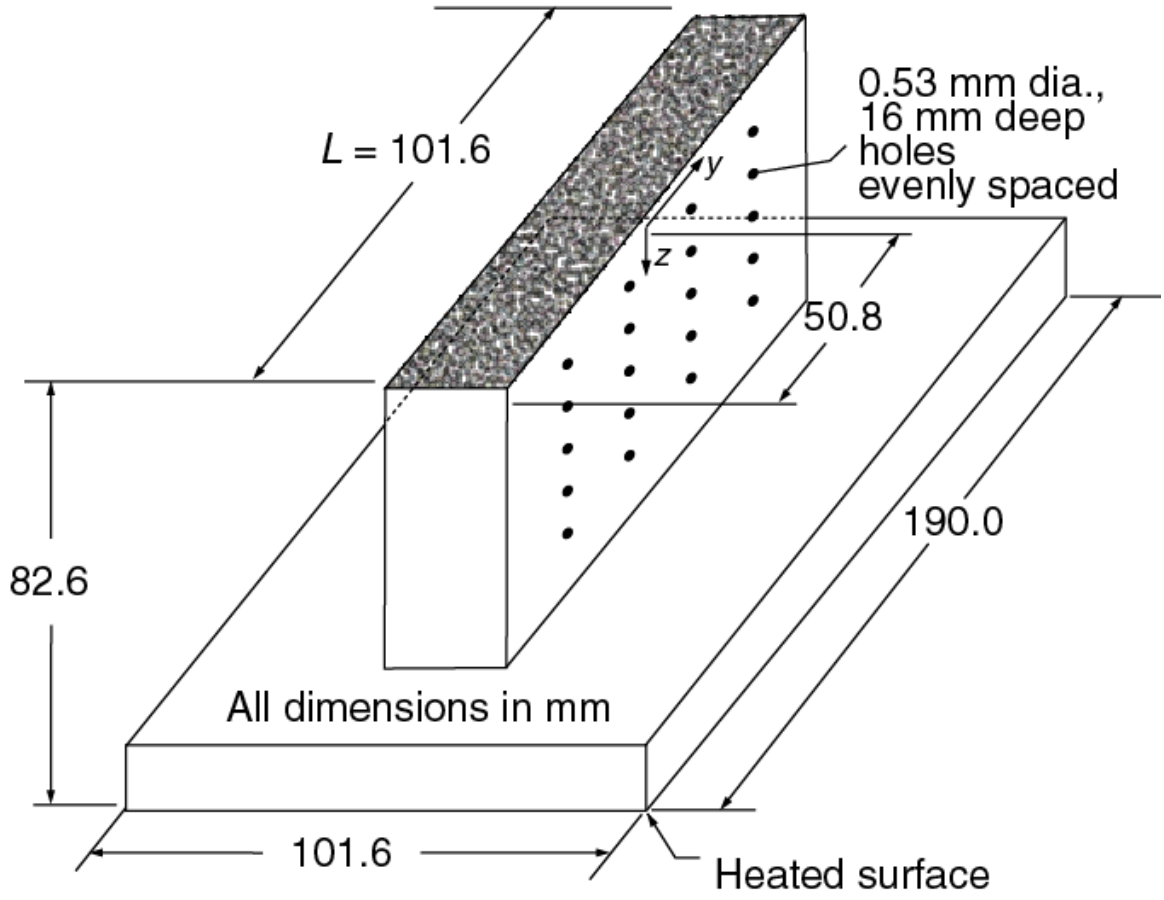

Fig. 2 OFHC copper flat test plate with Turbo-ESP surface and thermocouple coordinate system

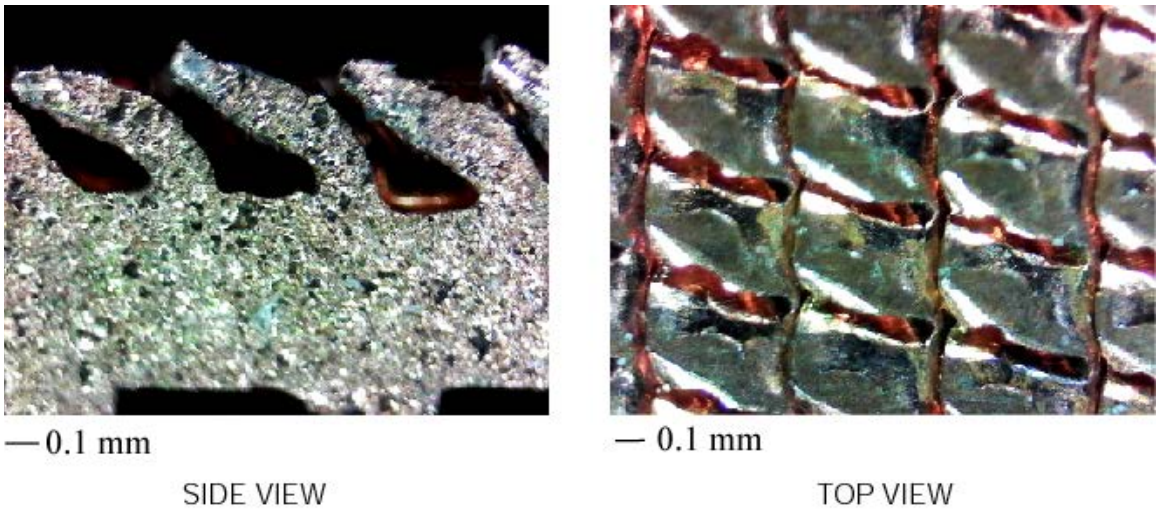

Fig. 3 Photograph of Turbo-ESP surface

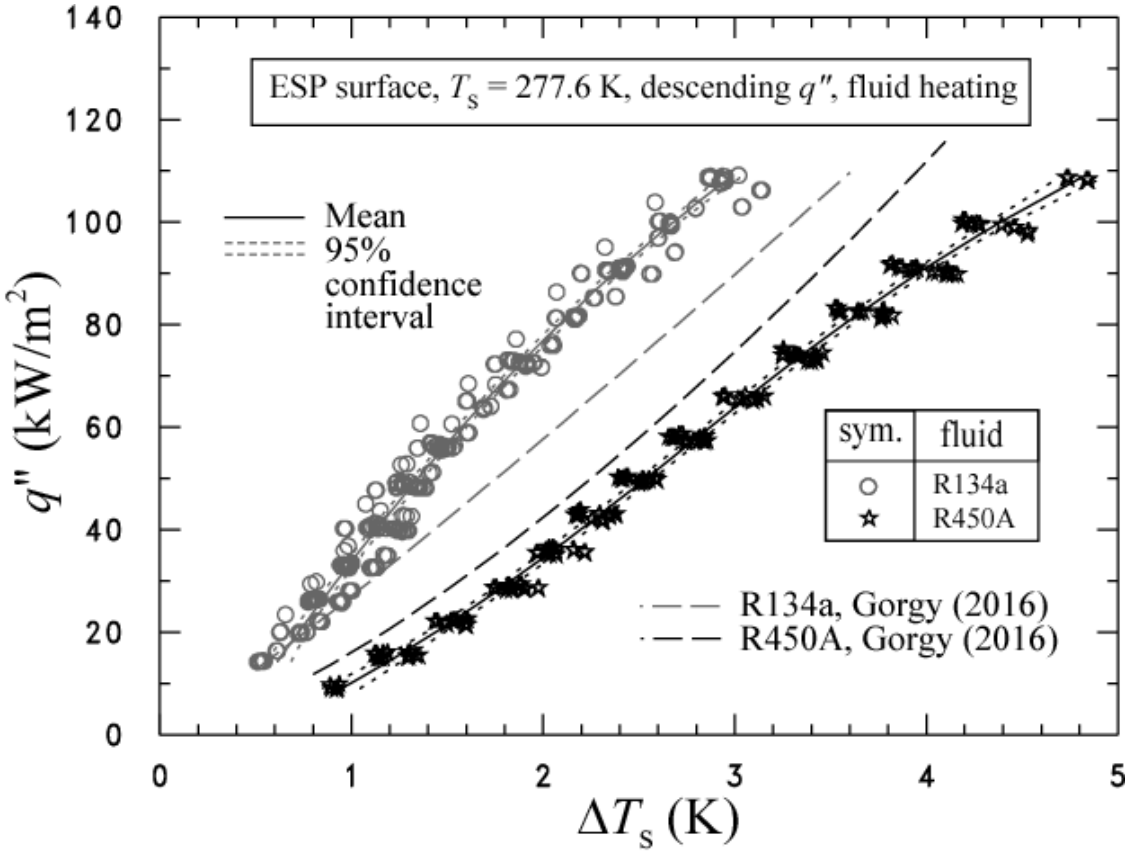

Fig. 4 Comparison of boiling curves for R134a and R450A on the Turbo-ESP surface to Gorgy (2016) measurements

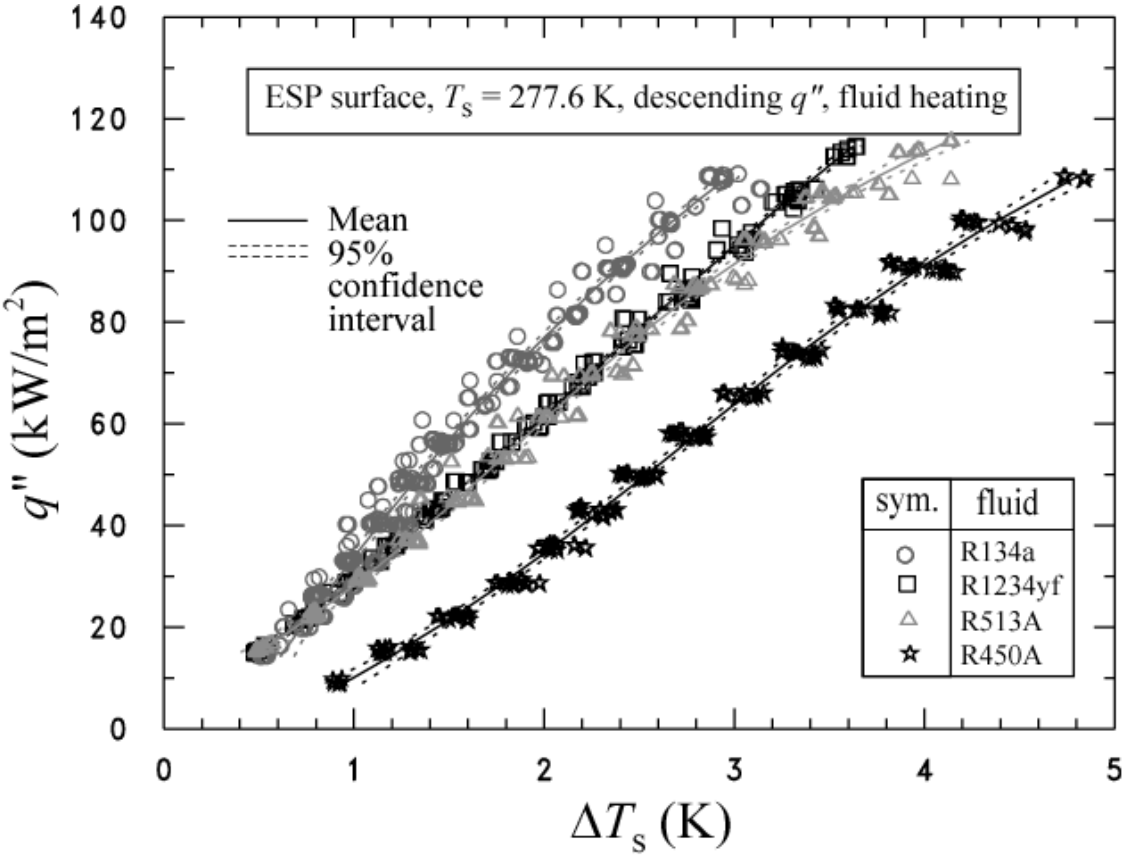

Fig. 5 Boiling curves for R134a and the low-GWP refrigerants for the Turbo-ESP surface

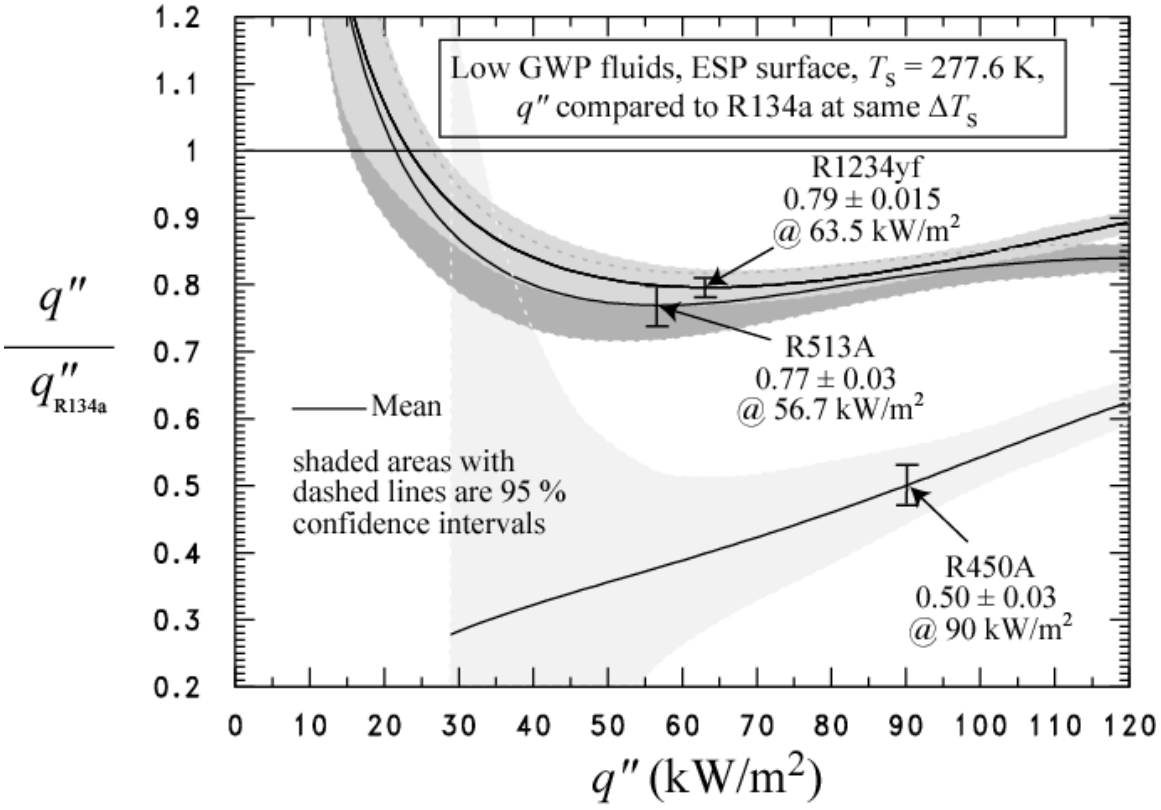

Fig. 6 Comparison of R134a heat flux on the Turbo-ESP surface to that for the low-GWP fluids at the same wall superheat

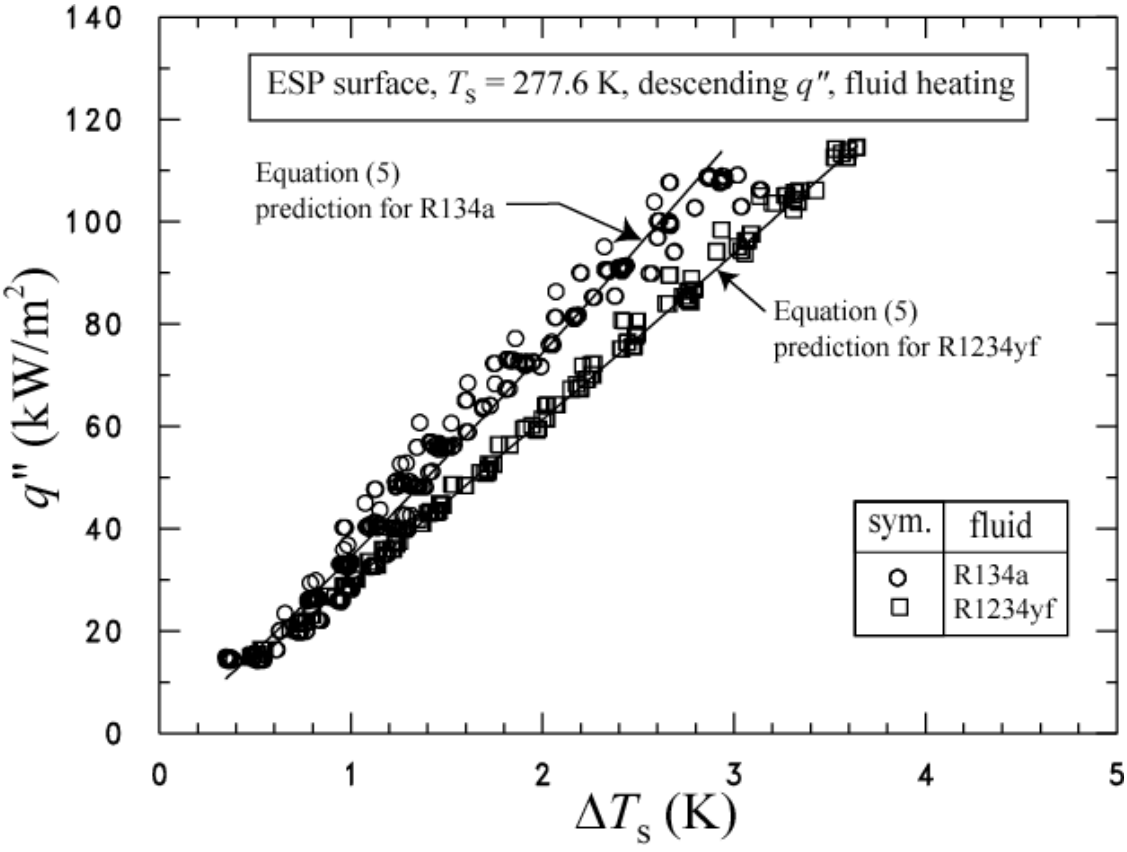

Fig. 7 Comparison of pool boiling model for Turbo-ESP surface for single component refrigerants to present measurements

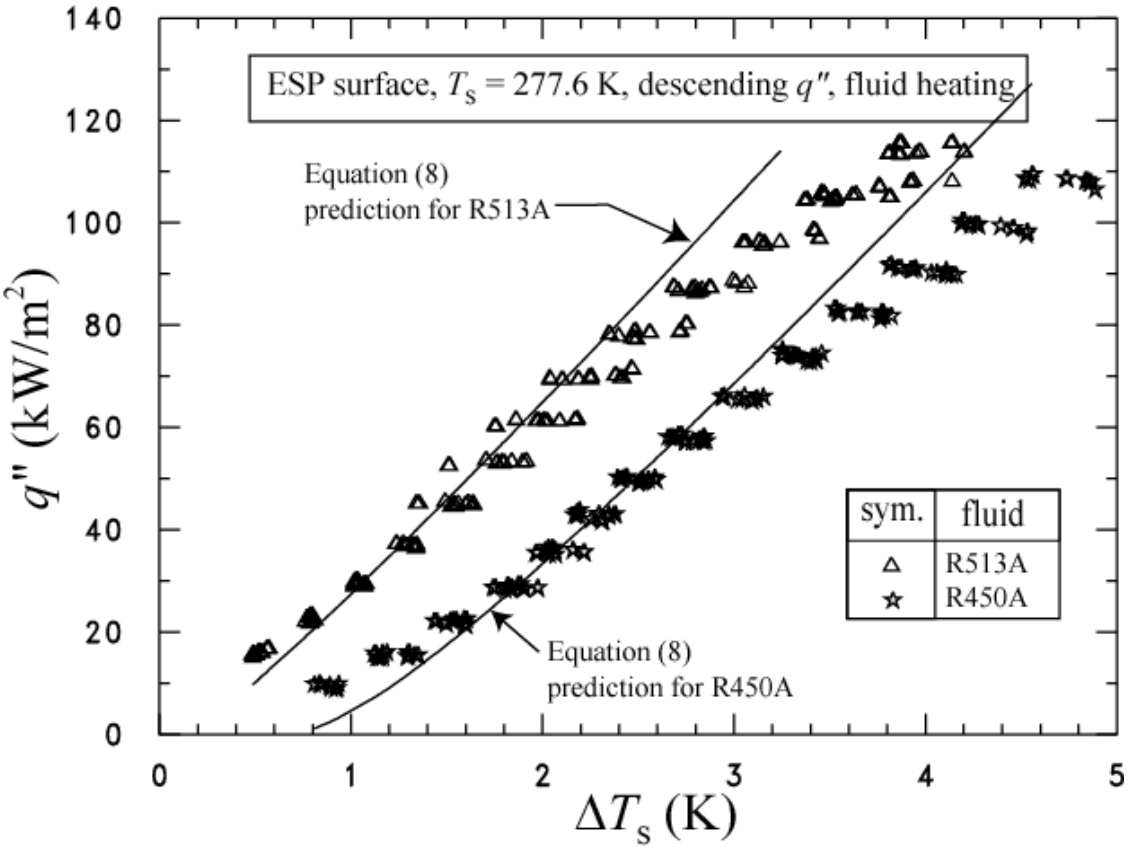

Fig. 8 Comparison of pool boiling model for Turbo-ESP surface for multi-component refrigerants to present measurements

APPENDIX A: UNCERTAINTIES

Figure A.1 shows the expanded relative (percent) uncertainty of the heat flux ($U_{q''}$) as a function of the heat flux. Figure A.2 shows the expanded uncertainty of the wall temperature as a function of the heat flux. The uncertainties shown in Figs. A.1 and A.2 are "within-run uncertainties." These do not include the uncertainties due to "between-run effects" or differences observed between tests taken on different days. The "within-run uncertainties" include only the random effects and uncertainties associated with one particular test. All other uncertainties reported in this study are "between-run uncertainties" which include all random effects such as surface past history or seeding.

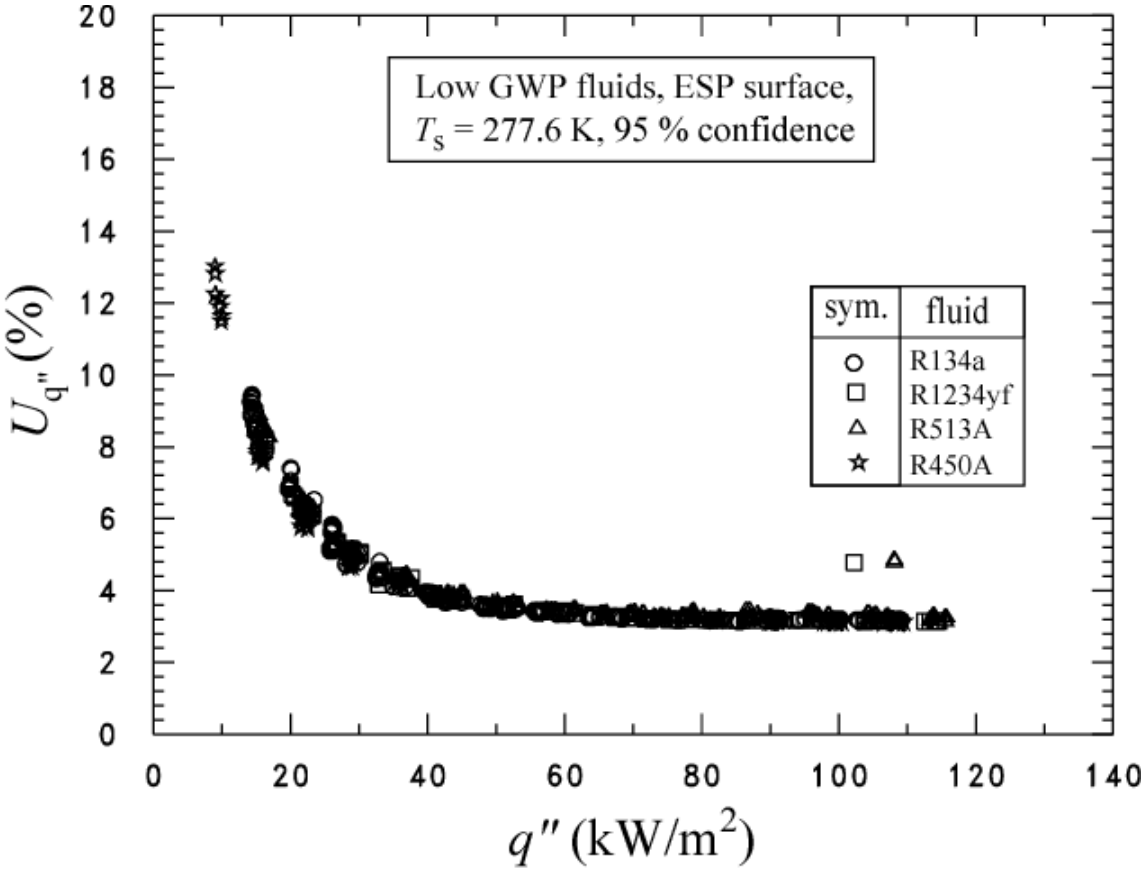

Fig. A.1 Expanded relative uncertainty in the heat flux of the surface at the 95 % confidence level

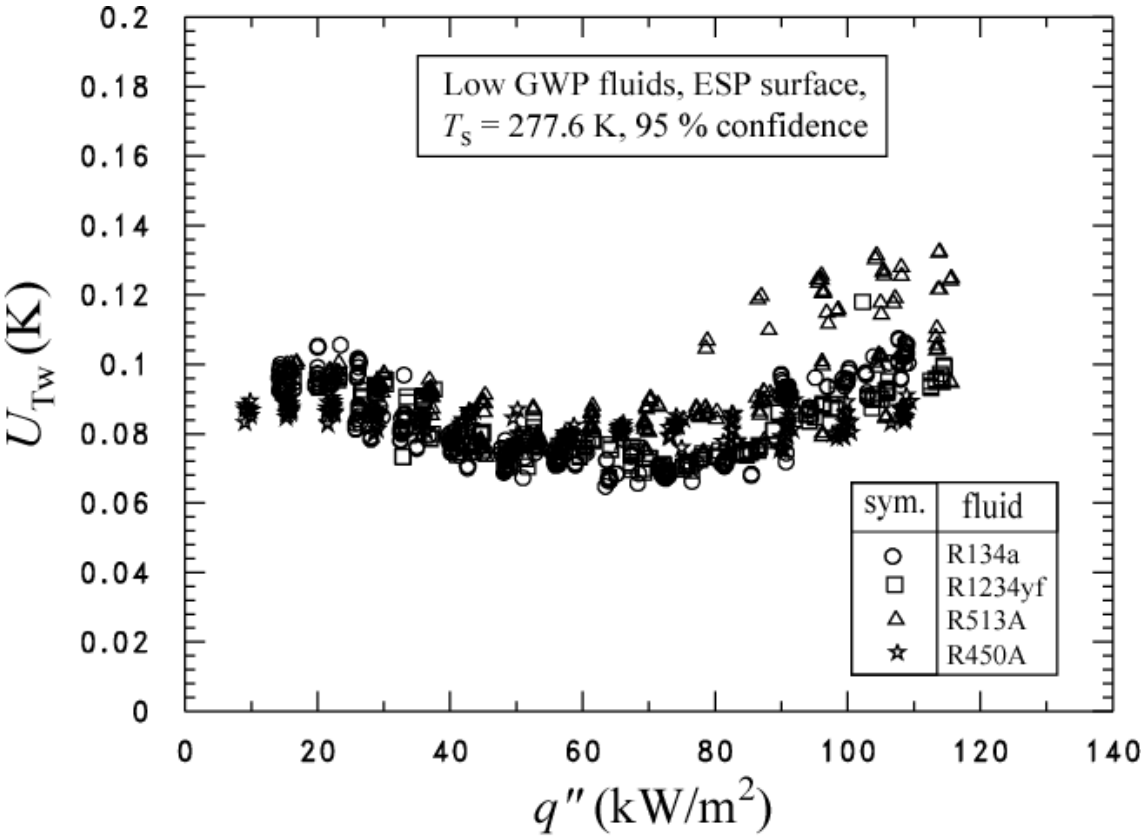

Fig. A.2 Expanded uncertainty in the temperature of the surface at the 95 % confidence level